Dynamics of Partial Wetting and Dewetting in Well-Defined Systems

Jordan G. Petrov,*,† John Ralston,‡ Matthew Schneemilch,§ and Robert A. Hayes‖

Institute of Biophysics of the Bulgarian Academy of Science, Str. Acad. G. Bonchev 1, Block 21, 1113 Sofia, Bulgaria, Ian Wark Research Institute, University of South Australia, Mawson Lakes, SA 5095, Australia, Department of Chemistry, Imperial College, Str. Kensington, London SW7 2AY, U.K., and Philips Research, Str. Prof. Holstlaan 4, 5656 AA Eindhoven, The Netherlands

By analyzing the assumptions of the hydrodynamic, molecular-kinetic and molecular-hydrodynamic theories of wetting dynamics, we formulated qualitative criteria for their applicability on the basis of the wetting−dewetting asymmetry of the dynamic contact angle/velocity dependence Θ/V presented on characteristic theoretical scales. The quantitative test concerns the physical plausibility of the values of the microscopic dynamic parameters obtained from the fit of the theoretical equations to experimental data. New Θ/V data were obtained and used to compare theory and experiment under well-defined conditions close to the assumptions of the theoretical models. The advancing and receding of methanol, ethanol, 1-butanol, and 1-octanol on the amorphous fluoropolymer AF 1600 were studied. The small AFM roughness ($0.3-0.4$ nm/μm^2), static angle hysteresis between 3 and 7°, and reproducibility within $\pm0.2°$ of the dynamic contact angles at different contact line positions demonstrate the good quality of the solid substrates. The use of pure liquids avoids complications with adsorption kinetics, and the low surface energy of the solid and the surface tension of the liquids minimize contamination effects. We found that the molecular-kinetic theory predicting a symmetry of advancing and receding branches of the cos Θ/Ca dependence works well at $Ca = \mu V/\gamma < \pm5 \times 10^{-4}$ but cannot explain the asymmetry at larger Ca values. The plot on the characteristic Θ^3/Ca scale shows that two-region hydrodynamic solutions work above $Ca = \pm2 \times 10^{-3}$ but do not describe the observed wetting−dewetting asymmetry. The same holds for the three-region solutions introducing the slip law or/and geometry of the system as numerical constants. The molecular-hydrodynamic theory fits the data over the whole Ca range studied and represents the wetting−dewetting asymmetry of the Θ/Ca plots. However, it gives inadequately small values of the molecular oscillation frequency K_0 unless the viscous friction in the contact line vicinity is not taken into account. Unreasonably small slip lengths $L_{S,max}$ and distances λ between the potential wells of the liquid molecules that are too large were obtained with all of the theories. They indicate shortcuts of the theoretical models for systems with partial wetting. At the same time, literature data for complete wetting confirm the Θ^3/Ca dependence and fluid interface shape predicted by the hydrodynamic theory.

I. Introduction

Wetting and dewetting phenomena include the advancing or receding of a liquid against a gas on a solid surface. This occurs during the deposition of coatings and paintings, spraying of pesticides and herbicides, and attachment of mineral particles to bubbles in froth flotation. After the establishment of equilibrium, the solid substrate is covered by a liquid film or by droplets. The first case is known as complete wetting, and the second one, as partial wetting. Although the dynamics of complete wetting is well understood, there are still unanswered questions about partial wetting.[1,2] They concern the nature and location of energy dissipation, the physical significance of the values of the microscopic dynamic parameters obtained from comparison of theory and experiment, the effect of geometry of the system, and so forth.

The motion of a fluid interface on a smooth, homogeneous, and nondeformable solid surface overcomes viscous friction in

the bulk of the liquid and nonhydrodynamic resistance located at the contact line. The majority of the theoretical studies[3−7] consider the balance between viscous friction and the capillary pressure gradient in the meniscus. Blake and Haynes[8] and Ruckenstein and Dunn[9] neglected the bulk viscous friction and evaluated the friction at the wetting perimeter by applying the Eyring molecular-kinetic theory of transport phenomena.[10] Combinations of the hydrodynamic and molecular-kinetic approach were also reported.[11−13] Zhou and Sheng[14] identified specific friction generated by the pinning of the moving contact line on solid surface defects. Shanahan and de Gennes[15] considered deformation of soft solid surfaces as another source of energy dissipation.

The theories of wetting dynamics introduce specific microscopic parameters that depend on the interactions in the three-phase contact zone. The hydrodynamic solutions[1−7] operate with slip lengths (L_S) or cutoff lengths (L_C) characterizing the dimensions of the region, where continuum hydrodynamics or its "no-slip" boundary condition fail. The molecular-kinetic theories[8,9] define a frequency K_0 of molecular oscillations between potential wells at the contact line and the distance λ between them. These parameters also appear in the combined

* Corresponding author. E-mail: jordan_g_petrov@yahoo.com.
† Bulgarian Academy of Science.
‡ University of South Australia.
§ Imperial College.
‖ Philips Research.

Partial Wetting/Dewetting in Well-Defined Systems

J. Phys. Chem. B, Vol. 107, No. 7, 2003 **1635**

molecular-hydrodynamic theory. However, the comparison of theory and experimental data for partial wetting often gives unreasonable values for L_S (or L_C), K_0, and λ.[16-20] One finds values of L_S between 10^{-12} and 10^{-3} cm, K_0 from 10^{-5} to 10^{10} s^{-1}, and λ significantly exceeding molecular dimensions. The subatomic slip or cutoff lengths, very small K_0, and λ values that are too high imply an inconsistency of the theoretical models or their inappropriate application.

These problems motivate us to carry out new experiments with well-defined solid surfaces and simple pure liquids. The values of L_S, K_0, and λ that are obtained for such systems should be more representative because they are being determined under conditions that are close to the assumptions of the theory. DuPont's amorphous fluoropolymers AF 1600 and AF 2400 offer good possibilities for such experiments. As for other fluoropolymers, they are chemically inert and have low surface energy. However, in contrast to PTFE, they are noncrystalline and can be dissolved in an appropriate fluorocarbon solvent at room temperature. This allows them to be cast as amorphous films on solid substrates. Such coatings are smooth; AFM images of AF 1600 cast on mica show a rms roughness of 0.3– 0.4 nm/μm^2 with several single features of 3–4 nm height.[21] Since mica does not introduce its own roughness, the above values characterize the AF 1600 surface. These properties result in a small contact angle hysteresis minimizing the problem by choosing an appropriate equilibrium contact angle. AF 1600- coated glass fibers showed $\Theta_A - \Theta_R = 4°$ for water and 6° for hexadecane[22,23] whereas on a conventional PTFE the same liquids exhibit hysteresis values of 22 and 18°, respectively (Figure 5 of ref 24).

The advantages of AF 1600 and AF 2400 have been utilized in several studies devoted to static contact angles and van der Waals interactions of dispersive liquids.[25] In our previous paper,[23] we obtained velocity dependencies of dynamic contact angles of nonpolar hexadecane and octamethylcyclotetrasiloxane on AF 1600. In the present investigation, we report Θ_{ext}/V data for methanol, ethanol, 1-butanol, and 1-octanol as examples of polar H-bonding liquids. The use of pure liquids avoids problems with adsorption kinetics at the solid–liquid and liquid–air interfaces. The low surface energy of the solid surface and low surface tension of the liquids minimize contamination effects. The static contact angles are between 60 and 70°, which enables both the wetting and dewetting mode to be studied under conditions of partial wetting. The predictions of the hydrodynamic, molecular-kinetic, and molecular-hydrodynamic theories regarding the symmetry of the wetting and dewetting modes were compared with the experimental data, and the values of the parameters obtained from the fit of theoretical equations were critically commented on.

II. Theoretical Models

Hydrodynamic Models. The hydrodynamic models consider two or three regions of the moving meniscus. In the outer region, capillary and gravitational forces balance each other, and the fluid interface obeys the Laplace equation. The inner region is located in close proximity to the contact line, where the liquid– liquid and liquid–solid interactions play a determining role. Conventional hydrodynamics encounters difficulties in this zone so that it is either ad hoc excluded[4] or the liquid is allowed to slip there to remove the viscous stress singularity arising from the "no-slip" boundary condition.[3,5] In the intermediate region separating the inner and outer zones, viscous and capillary forces determine the hydrodynamics and the shape of the fluid interface. At small contact angles, disjoining pressure can also

play a role in this part of the meniscus.[6] The geometry of the system affects the fluid interface profile in the outer region but does not influence the shape of the inner and intermediate regions.[4,5]

By directly matching the inner and outer regions, Dussan[3] obtained a two-region solution for $Ca \rightarrow 0$ that is correct to order Ca^0:

$$G(\Theta_{m,0}) = G(\Theta_c) + Ca \ln\left(\frac{L_H}{L_S}\right) \qquad (1)$$

$$G(\Theta) \equiv \int_0^\Theta \frac{\beta - \sin\beta\cos\beta}{2\sin\beta} \, d\beta$$

The macroscopic dynamic contact angle $\Theta_{m,0}$ in eq 1 corresponds to a quasi-static meniscus shape and can be measured via all methods utilizing static relationships between the contact angle and, for example, the apex height, main radius of curvature, capillary pressure, meniscus weight, and so forth. The microscopic dynamic angle Θ_c is the slope of the fluid interface in the inner region. The slip length L_S designates the size of the inner region, and L_H is a characteristic dimension of the flow in the outer region.

By matching the asymptotic solutions for the inner, intermediate, and outer regions, Cox[5] solved the hydrodynamic problem for two immiscible fluids displacing each other on a solid wall. When one of the fluids is a gas, his result, correct to order Ca^{+1}, reads

$$G(\Theta_m) = G(\Theta_c) + Ca\left[\ln\left(\frac{L_H}{L_S}\right) + \frac{Q_{in}}{f(\Theta_c)} - \frac{Q_{out}}{f(\Theta_m)}\right] \quad (2)$$

Equation 2 is valid for $Ca \rightarrow 0$, $L_S/L_H \rightarrow 0$, and $Ca \ln(L_H/L_S)$ ≈ 1. Here, the macroscopic dynamic contact angle Θ_m represents the boundary condition of the outer region at its end or at the contact line. Q_{in} is an integration constant of the fluid interface profile in the inner region that depends on μ, Θ_c, and the particular slip law. Q_{out} is the integration constant for the profile of the outer region; it is a function of μ, Θ_m, and the geometry of the system.

Zhou and Sheng[14] found that different slip models yield the same $\Theta_{m,0}/Ca$ relationship if the slip length is normalized by a constant K_{ZS} that is specific to the given slip model:

$$G(\Theta_{m,0}) = G(\Theta_c) + Ca \ln\left(\frac{L_H}{L_S/K_{ZS}}\right) =$$

$$G(\Theta_c) + Ca\left[\ln\left(\frac{L_H}{L_S}\right) + C_{ZS}\right] \quad (3)$$

Voinov[4,26] excluded the tip of the meniscus at a cutoff distance L_C and matched the solutions for the intermediate and outer regions for small drops, narrow slots, and thin capillaries where gravity is negligible. He found that one could account for the geometry of such systems through a numerical constant K_V that normalizes the dimension of the macroscopic hydrodynamic flow L_H:

$$\Theta_{ext}^3 = \Theta_c^3 + 9Ca \ln\left(\frac{L_H/K_V}{L_C}\right) = \Theta_c^3 + 9Ca\left[\ln\left(\frac{L_H}{L_C}\right) - C_V\right] \quad (4)$$

Equation 4 is an approximation that is valid for contact angles between 30 and 135°. For drops, L_H should be substituted by their maximum height with $C_V = 1.0$; for slots, L_H is the half-

1636 *J. Phys. Chem. B, Vol. 107, No. 7, 2003*

Petrov et al.

width of the slot, and $C_V = 1.5$; for capillaries, L_H represents their radius, and $C_V = 1.8$. θ_{ext} is defined by the slope at the solid wall of the extrapolated quasi-static part of the moving meniscus, which coincides with the Cox definition[5] of the macroscopic dynamic contact angle θ_m.

Voinov[4,26] found that if $\Theta < 150°$, then $G(\Theta) \approx \Theta^3/9$ with 1% accuracy. For such contact angles, eqs 1–3 become

$$\Theta_{m,0}^3 = \Theta_c^3 + 9Ca \ln\left(\frac{L_H}{L_C}\right) \tag{1a}$$

$$\Theta_{ext}^3 = \Theta_c^3 + 9Ca\left[\ln\left(\frac{L_H}{L_S}\right) + \frac{Q_{in}}{f(\Theta_c)} - \frac{Q_{out}}{f(\Theta_m)}\right] \tag{2a}$$

$$\Theta_{ext}^3 = \Theta_c^3 + 9Ca\left[\ln\left(\frac{L_H}{L_C}\right) + C_{ZS}\right] \tag{3a}$$

By unifying the Voinov and Zhou-Sheng approaches, we can combine eqs 3a and 4 for $L_S \approx L_C$:

$$\Theta_{ext}^3 = \Theta_c^3 + 9Ca\left[\ln\left(\frac{L_H}{L_S}\right) + C_{ZS} - C_V\right] \tag{5}$$

Equations 5 and 2a are rather similar, with C_{ZS} staying for $Q_{in}/f(\Theta_c)$ and C_V, for $Q_{out}/f(\Theta_m)$. However, C_{ZS} and C_V are numerical constants whereas the second and third terms in eq 2 depend on the material properties of the system via μ and might vary with Ca because $f(\Theta_c)$ and $f(\Theta_{ext})$ depend on the contact line velocity.

Using the Voinov simplification, one can present all of the above hydrodynamic equations (eqs 1–5) in the same mathematical form:

$$\Theta^3 = \Theta_c^3 + 9CaH \tag{6}$$

Here, Θ stays for $\Theta_{m,0}$ or Θ_{ext}, and H represents the corresponding expression in brackets. Since the values of L_H and L_S for wetting and dewetting cannot differ by orders of magnitude, $H = \ln(L_H/L_S)$ and $d\theta_{m,0}^3/dCa$ in eq 1a should be practically the same for $Ca > 0$ and $Ca < 0$. Such symmetry could serve as a qualitative check of the two-region hydrodynamic model. By determining H from $\theta_{m,0}/Ca$ data, one could evaluate L_S if L_H is known for the given system. Such a specification is difficult, but we can estimate the maximum possible value of L_S by substituting L_H with the maximum possible dimension of the outer region (e.g., the maximum meniscus or drop height, capillary radius, half-width of the slot, and so forth).

$$L_{S,max} = L_{H,max} \exp\left(-\frac{d\Theta_{m,0}}{9\,dCa}\right) \tag{7}$$

For eqs 2a, 3a, 4, and 5, H contains two or three unknown quantities. According to eq 3a, the $\theta_{m,0}^3/Ca$ dependence would be asymmetric if C_{ZS} has a different sign and/or value for wetting and dewetting. Equations 4 and 5 would predict asymmetric advancing and receding θ_{ext}^3/Ca branches if C_V and $C_{ZS} - C_V$, respectively, depend on the direction of the contact line motion.

The above theories assume that Θ_c is a constant that is represented by the Young angle Θ_Y in ideal systems. For real surfaces, Cox[5] recommends using the effective equilibrium angle defined by Wenzel[27] or Cassie[28] the maximum static advancing angle $\Theta_{A,max}$, or the minimum static receding $\Theta_{R,min}$ contact angle. Independent of this choice, all hydrodynamic equations predict a linear Θ^3/Ca relationship if $\Theta_c =$ a constant.

Alternative to the above assumption is a dependence of Θ_c on the contact line velocity, which implies an additional frictional force F_c at the contact line. Previous studies suggest[14,45] that $F_c \approx BCa^n$ with $0 < n < 0.5$, which yields

$$\cos\Theta_c = \cos\Theta_0 \mp BCa^n \tag{8}$$

The "−" stays for wetting, and the "+", for dewetting. Because of the noninteger power, Ca must be taken to be positive for both modes. Zhou and Sheng substituted eq 8 into eq 1, thus accounting for both bulk viscous and contact line friction. Here, we combine eqs 4 and 8 to introduce the systems' geometry via the Voinov constant C_V. This combination utilizes the extrapolated dynamic angle Θ_{ext} instead of $\Theta_{m,0}$:

$$\Theta_{ext,adv}^3 = [\arccos(\cos\Theta_0 - BCa^n)]^3 + 9Ca\left[\ln\left(\frac{L_H}{L_S}\right) + C_{ZS} - C_V\right] \tag{9a}$$

$$\Theta_{ext,rec}^3 = [\arccos(\cos\Theta_0 + BCa^n)]^3 - 9Ca\left[\ln\left(\frac{L_H}{L_S}\right) + C_{ZS} - C_V\right] \tag{9b}$$

Zhou and Sheng[14] ascribed the contact line friction to its pinning at defects of the solid surface. They found a dependence of B on the distance between defects $L_d = L_j/b$, jump length L_j, surface tension γ, density ρ, and viscosity μ of the liquid (b is a numerical constant >1):

$$B = 1.3b\left(\frac{\pi^3\gamma\rho L_d}{\mu^2}\right)^{1/2} \tag{10}$$

Equation 10 reflects the particular mechanism proposed in ref 14, but eqs 9a and 9b are rather general if one does not specify the physical meaning of the numerical constants B and n.

Molecular-Kinetic Models. Blake and Haines[8] and Ruckenstein and Dunn[9] developed a molecular-kinetic theory that postulates that the entire energy dissipation is located at the contact line. This assumption implies that the whole moving meniscus obeys the Laplace equation. Under such conditions, the macroscopic dynamic contact angle Θ has a rigorous definition and can be measured by all static methods.

The Blake–Haynes theory[8] considers an ideal solid surface with randomly distributed monoenergetic adsorption centers at a mean distance λ. At equilibrium, the molecules at the contact line oscillate between the centers at the solid–gas and solid–liquid interfaces with frequency $K_0 = (kT/h) \exp(-\Delta g_0/kT)$ determined by the activation free energy Δg_0 and temperature T. Under dynamic conditions, the net frequency is $K = K^+ - K^-$, where K^+ and K^- are the number of jumps per second in the direction of motion and in the opposite direction.

The contact line motion is driven by the unbalanced Young force $\gamma[\cos\Theta_Y - \cos\Theta(V)]$. This theory assumes that this force decreases the equilibrium activation free energy Δg_0 in the forward direction and increases it in the backward direction by the *same* quantity $\Delta g/2$:

$$K^+ = \frac{kT}{h}\left[\exp\left(-\frac{\Delta g_0 - \Delta g/2}{kT}\right)\right] \tag{11a}$$

$$K^- = \frac{kT}{h}\left[\exp\left(-\frac{\Delta g_0 + \Delta g/2}{kT}\right)\right] \tag{11b}$$

The free-energy change Δg associated with contact line motion

Partial Wetting/Dewetting in Well-Defined Systems

J. Phys. Chem. B, Vol. 107, No. 7, 2003 **1637**

is related to the driving force $\Delta g = \gamma \lambda^2 (\cos \Theta_Y - \cos \Theta)$. By introducing this relationship in eqs 11a and 11b and combining them with the definition[29] of the mean velocity of a unit length of the contact line $V = K\lambda$, one obtains the Blake−Haynes relationship:

$$\cos \Theta = \cos \Theta_Y - \frac{2kT}{\gamma \lambda^2} \text{arsh}\left(\frac{V}{2K_0\lambda}\right) \qquad (12)$$

The same value of Δg for the advancing and receding motions of the contact line postulates unique values of Θ_Y, λ, and K_0 for a given system that is invariant to the direction of the contact line motion. This fact is expressed by the symmetric arsh function in eq 12, which requires symmetric advancing and receding branches of the $\cos \Theta/V$ dependence. This feature could be used as a qualitative test of the molecular-kinetic theory.

Blake and Haynes[8] were aware that their model "implies that the same amount of work is done on each site irrespective of whether it is initially occupied by a molecule of phase 1 or one of phase 2." Unfortunately, most of the following papers applying their theory neglected this remark. They dealt either with wetting or dewetting, or where both modes were investigated, the advancing and receding Θ/V branches were fitted separately.[16,17,30,32] To the best of our knowledge, the only exceptions are refs 22 and 32, but the latter study reports a strange low value of $K_0 = 8 \times 10^{-5}$ s^{-1} for one of the systems.

Molecular-Kinetic Models Accounting for Contact Line and Viscous Dissipation. Following Cherry and Holms,[33] Blake[30] related the viscosity of the liquid in the zone adjacent to the contact line to the activation free energy of the viscous flow $\Delta g_{0,v}$:

$$\mu = \frac{h}{\nu} \exp \frac{\Delta g_{0,v}}{kT} \qquad (13)$$

For simple Newtonian liquids, ν is the molecular volume. He presented the total activation free energy $\Delta g_{0,w}$ as the sum of a surface and a viscous component, $\Delta g_{0,w} = \Delta g_{0,s} + \Delta g_{0,v}$ and introduced a complex wetting−dewetting frequency $K_{0,W} = (kT/h) \exp(-\Delta g_{0,w}/kT)$. The latter two expressions and eq 13 relate $K_{0,W}$ to the equilibrium oscillation frequency at the contact line $K_{0,S}$ and the viscosity of the liquid:

$$K_{0,W} = \frac{kT}{h} \exp\left(-\frac{\Delta g_0}{kT}\right) = K_{0,S}\left(\frac{h}{\mu \nu}\right) \qquad (14)$$

Furthermore, Blake followed the approach described in the former section, assuming that the λ values at the contact line and in the liquid phase are the same. This gave[30]

$$\cos \Theta = \cos \Theta_Y - \frac{2kT}{\gamma \lambda^2} \text{arsh}\left(\frac{\mu \nu V}{2K_{0,S}\lambda h}\right) \qquad (15)$$

The more complex version of the molecular-kinetic theory also neglects the viscous bending of the fluid interface and postulates a quasi-static meniscus profile.

It is easy to see that eqs 12 and 15 can be written in the same mathematical form:

$$\cos \Theta = \cos \Theta_Y - \frac{2kT}{\gamma \lambda^2} \text{arsh}\left(\frac{Ca}{C_B}\right) \qquad (16)$$

Here we introduce the Blake constant C_B. For the simple molecular-kinetic theory, $C_B = 2K_{0,S}\lambda/(\gamma/\mu)$, and for its more general version, $C_B = 2K_{0,S}\lambda/(\gamma \nu/h)$. Thus, the symmetry of the $\cos\Theta$ versus Ca dependence for wetting ($Ca > 0$) and dewetting

($Ca < 0$) is predicted by both versions, and this feature can serve as a qualitative test of both molecular-kinetic models.

Combined Molecular-Hydrodynamic Models. De Gennes[1] emphasized the fact that in the case of partial wetting the total dissipation could include both the bulk viscous dissipation and the nonviscous dissipation at the moving contact line. Brochard-Wyart and de Gennes[12] analyzed the components of the total dissipative force F_D:

$$F_D = \frac{3\mu V \ln(X_{max}/X_{min})}{\Theta} + C \qquad (17)$$

The first term on the right-hand side represents the hydrodynamic contribution, and the second one stays for the contact line friction. X_{max} and X_{min} are the macroscopic and microscopic cutoff lengths, specified above as L_H and L_C (or L_S), respectively. The coefficient of the contact line friction C was estimated from the Blake−Haynes theory that was linearized for small driving forces:

$$C = \frac{kT}{K_{0,S}\lambda^3} = \frac{h}{\lambda^3} \exp\left(\frac{\Delta g_{0,S}}{kT}\right) \qquad (18)$$

If the activation energy of the molecular hopping at the contact line $\Delta g_{0,S}$ is comparable with the one determining the viscosity of the liquid $\Delta g_{0,V}$, then the prevalence of one of the right-hand-side terms will depend on the dynamic contact angle Θ. For small Θ, the viscous friction term will predominate, large dynamic angles implying more-significant nonhydrodynamic friction.[12]

Voinov[4] analyzed the energy conservation during the wetting process. The free-energy change ΔG_s caused by the transposition of the contact line plus the work W_p done by the capillary pressure should be equal to the sum of the energy dissipation at the contact line E_c and the bulk viscous energy dissipation E_v. The bulk quantities W_p and E_v were evaluated for large contact angles by applying the creeping-flow model to the intermediate region. The latter was assumed to be planar so that the capillary pressure work W_p could be neglected. The remaining components of the energy conservation equation gave the relationship between the microscopic contact angle Θ_c and the contact line frictional force F_c:

$$\cos \Theta_Y - \cos \Theta_c(V) = \frac{F_c}{\gamma} \qquad (19)$$

The microscopic energy dissipation E_c should be a positive function of the absolute contact line velocity $E_c \approx G|V|$ that might differ for wetting ($V > 0$) and dewetting ($V < 0$). The microscopic frictional force F_c would also then be asymmetric. Brochard-Wyart and de Gennes[12] as well as Petrov and Petrov[13] considered the symmetric case, but the latter authors substituted F_c by the nonlinearized Blake−Hayes expression:

$$F_c = \frac{2kT}{\lambda^2} \text{arsh}\left(\frac{V}{2K_{0,S}\lambda}\right) \qquad (20)$$

Equations 19 and 20 give the relationship between Θ_c and V. Its incorporation into eq 4 formulates the combined molecular-hydrodynamic theory that accounts for the nonhydrodynamic friction at the contact line and the viscous friction in the intermediate region of the meniscus. Voinov constant C_V formally represents the geometry of the system:

$$\Theta_{ext} = \left\{ \Theta_c^3(V) + 9\frac{\mu V}{\gamma}\left[\ln\left(\frac{L_{0,R}}{L_C}\right) - C_V\right]\right\}^{1/3} \quad (21a)$$

$$\Theta_c(V) = \arccos\left[\cos\Theta_Y - \frac{2kT}{\gamma\lambda^2}\text{arsh}\left(\frac{V}{2K_{0,S}\lambda}\right)\right] \quad (21b)$$

We substitute L_H by the maximum static meniscus height $L_{0,R}$, which depends on fiber radius R.

The frictional force F_c at the contact line and in the inner region can be represented by the more complex Blake expression:[34]

$$F_c = \frac{2kT}{\lambda^2}\text{arsh}\left(\frac{\gamma v/h}{2K_{0,S}\lambda}Ca\right) \quad (22)$$

Combining eqs 4, 19, and 22 gives

$$\Theta_{ext} = \left\{\Theta_c^3(Ca) + 9Ca\left[\ln\left(\frac{L_{0,R}}{L_C}\right) - C_V\right]\right\}^{1/3} \quad (23a)$$

$$\Theta_c(Ca) = \arccos\left[\cos\Theta_Y - \frac{2kT}{\gamma\lambda^2}\text{arsh}\left(\frac{\gamma v/h}{2K_{0,S}\lambda}Ca\right)\right] \quad (23b)$$

Equations 23a and 23b formulate a more general molecular-hydrodynamic theory. Both versions represented by eqs 21a and 21b and eqs 23a and 23b can be presented in the same mathematical form:

$$\Theta_{ext} = \left[\Theta_c^3(Ca) + 9Ca\left(\ln\frac{L_{0,R}}{L_C} - C_V\right)\right]^{1/3} \quad (24a)$$

$$\Theta_c(Ca) = \arccos\left[\cos\Theta_Y - \frac{2kT}{\gamma\lambda^2}\text{arsh}\left(\frac{Ca}{C_B}\right)\right] \quad (24b)$$

Equation 24b should be read with $C_B = 2K_{0,S}\lambda/(\gamma/\mu)$ for the simple molecular-hydrodynamic theory and with $C_B = 2K_{0,S}\lambda/(\gamma v/h)$ for its more general version. The unknown parameters λ, $K_{0,S}$, and $H = \ln(L_{0,R}/L_C) - C_V$ can be determined from the fit to the experimental Θ_{ext}/Ca data. Since Voinov constant C_V varies between 1.0 and 1.8 for small drops, narrow slots, and capillaries, one could expect a similar value for thin fibers. For real surfaces, Θ_Y should be substituted by an effective Young angle Θ_0 because the molecular-kinetic theory (eq 24b) requires a unique static angle for a given system. Here we follow Adam[35] and more recent investigations[36,37] that determine Θ_0 from the maximum advancing $\Theta_{A, max}$ and the minimum receding static contact angle $\Theta_{R, min}$:

$$\cos\Theta_0 = \frac{\cos\Theta_{A,max} + \cos\Theta_{R,min}}{2} \quad (25)$$

This approach differs from the application of dynamic contact angles recorded at small velocities to characterize the solid surface energetics.[38] For such purposes, the advancing contact angle could be more appropriate because the receding angle could be affected by the sorption of the liquid.

III. Experimental Section

Materials and Methods. The investigated fluoropolymer surfaces were obtained via dip-coating silica optical fibers with a radius of 60 μm. The clean fibers were immersed to a depth of 4 cm at a speed of 0.5 cm/s in a 1% w/v solution of AF 1600 in FC75 (3M fluorocarbon solvent) and withdrawn at the same speed after 1 min. The solvent was allowed to evaporate in a laminar flow cabinet for 1 h. The coating thus obtained

TABLE 1: Properties of the Liquids Used

property	CH_3OH	C_2H_5OH	C_4H_9OH	$C_8H_{17}OH$
surface tension, γ [mN/m]	22.2	22.1	25.0	27.2
density, ρ [g/cm^3]	0.791	0.789	0.810	0.827
viscosity, μ [cP]	0.564	1.13	2.75	7.61
molecular volume, $v = M/\rho N_A$ [cm^3/molecule]	6.72×10^{-23}	9.69×10^{-23}	1.519×10^{-22}	2.614×10^{-22}
characteristic hydrodynamic velocity, γ/μ [cm/s]	3936	1954	907	357
purity [%]	99.8	99.8	99.8	99
supplier	Aldrich	Fluka	Aldrich	Aldrich

TABLE 2: Characteristics of the Static Wetting of AF 1600 by the Liquids Used

property	CH_3OH	C_2H_5OH	C_4H_9OH	$C_8H_{17}OH$
static advancing contact angle, Θ_A [deg]	68.9	62.8	68.3	74.4
static receding contact angle, Θ_R [deg]	66.0	59.7	63.8	67.1
static contact angle hysteresis, $\Theta_A - \Theta_R$ [deg]	2.8	3.1	4.5	7.3
effective equilibrium contact angle, Θ_0 (eq 25) [deg]	67.4	61.3	66.1	70.8
maximum static capillary height, $L_{0,R}(\Theta_{R(A)} = 0°)$ [cm]	0.0252	0.0252	0.0255	0.0257

was better than that on large plates or cylinders. This difference and the necessity to work with long samples to achieve a steady state at high velocity determined our choice of fibers as solid substrates.

Methanol, ethanol, 1-butanol, and 1-octanol were used as received from the suppliers. Their properties, taken from the literature, are given in Table 1. They have a low surface tension γ that slightly increases from methanol to octanol and a low viscosity μ that increases more significantly in the same direction. Representative of their hydrodynamic properties is the characteristic velocity γ/μ at which viscous effects become significant. This quantity normalizes the speed of the fluid interface giving the capillary number. Table 1 shows that γ/μ decreases by an order of magnitude from methanol to octanol.

Table 2 shows the static advancing and receding contact angles, Θ_A and Θ_R, respectively, determined 1 min after stopping the dipping or withdrawing the fiber. The static hysteresis $\Theta_A - \Theta_R$ that characterizes the solid-surface non-ideality is small for all liquids. The effective equilibrium contact angle Θ_0 evaluated from eq 25 does not change systematically. The maximum static capillary height $L_{0,R}$ at which $\Theta_{A(R)} = 0°$ (determined from the numerical solution of the Laplace equation) is practically the same for all liquids.

The optical method described below enables the determination of the extrapolated dynamic contact angle Θ_{ext} in eqs 2, 4, 5, 9, 21, 23, and 24. This quantity is rigorously defined and can be accurately measured in the presence of the viscous deformation of the meniscus. For a quasi-static fluid interface, the same procedure yields $\Theta_{m,0}$, which stays in eqs 1 and 3. Usually, 20 steady values of θ_{ext} were averaged, giving a scatter below 0.5° at low and moderate velocities. Since each value corresponds to a different position of the contact line along the fiber, such
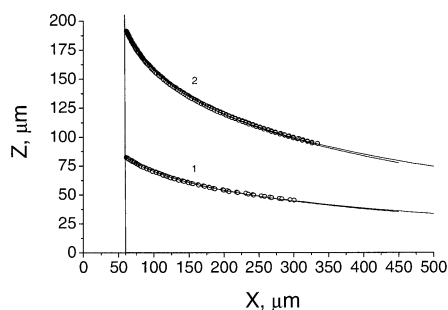
Partial Wetting/Dewetting in Well-Defined Systems

J. Phys. Chem. B, Vol. 107, No. 7, 2003 **1639**

Figure 1. Profiles of the octanol−air interface under (1) static and (2) dynamic conditions. The vertical line represents the solid wall. The upper solid lines correspond to numerical fits of the Laplace equation, and the lower one, to fits of the Derjaguin equation. The Laplacian fit of curve 1 gives $\theta_R = 67.8°$, and the Derjaguin fit yields $\theta_R = 67.7°$. Curve 2 gives the smallest dynamic contact angles in this study, $\theta_{\text{ext,Lpc}} = 33.6°$ and $\theta_{\text{ext,Drg}} = 33.4°$.

reproducibility demonstrates the good quality of the surfaces used in this study.

The entire apparatus was suspended with elastic rope within an enclosed cabinet to minimize the influence of vibration and air currents. The AF 1600-coated fiber was suspended vertically from a motorized stage (Time and Precision, Basingstoke, U.K.) with a screw having a pitch of 2 mm. It was dipped or withdrawn from a liquid bath at velocities ranging from 2 μm/s to 2 cm/s. The measurements were performed in "overfilled" beakers because all of the static and dynamic contact angles that were studied were below 90°. A backlit Köhler source gave collimated light projecting a silhouette of the meniscus profile. Because of the fiber's curvature, there were no reflections from the solid surface affecting the background intensity close to the contact line. This gave consistently high contrast up to the solid wall, improving the precession of the method. Imaging of the meniscus was conducted with a 5× long-working-distance objective lens and a 6.7× field lens giving such a magnification that half of the fiber and the meniscus occupied the full screen width. Video images were captured with a Sony Iris CCD camera and stored on VHS tape before the digitization of appropriate frames. Twenty frames on average were selected from the footage of the interface after the steady state had been reached. Since the maximum acceleration was limited (5 cm/s^2), the advancing images were taken close to the top of the fiber, and the receding images were taken at the bottom of the fiber. The frames were converted to 256 gray-level images with a pixel resolution of approximately 1 μm. A graticule with 20-μm gradations was used to calibrate the images in the X and Y directions. The location of the interface was determined from the positions of the outermost image pixels with gray-level values below 80. The position of the interface determined using this threshold value coincided with the location of pixels with a maximum gray-level gradient calculated from a 5 × 5 matrix.

The coordinates of the fluid interface Z, X were fitted by a numerical solution of the Laplace equation using the algorithm detailed by Huh and Scriven.[39] The analytical solution of Derjaguin,[40] valid with 1% accuracy for thin fibers with $R < 0.1a$, was also applied as in our previous study:[41]

$$Z = R \cos \Theta_{\text{ext}} \left[0.462 + \ln \left(\frac{a}{X + \sqrt{X^2 - R^2 \cos^2 \Theta_{\text{ext}}}} \right) \right] \quad (26)$$

The two fitting procedures produce overlapping profiles down to 300 μm from the solid wall. At the maximum capillary number (Figure 1, profile 2), they give extrapolated contact angles differing by less than 0.2°. This value is close to the error of determination of θ_{ext}.

Viscous Deformation of the Moving-Fluid Interface. The experimental conditions of this study correspond to small capillary and Bond numbers ($Ca \leq 5.6 \times 10^{-3}$, $Bo \leq 2.2 \times 10^{-2}$), implying small macroscopic viscous effects and a small gravity contribution. Figure 1 shows two profiles of the octanol−air interface recorded under (1) static and (2) dynamic conditions. The upper solid lines correspond to the numerical fit of the Laplace equation, and the lower ones, to the Derjaguin expression. Although both fits utilize "static equations", they follow the experimental coordinates up to the solid wall. Profile 2 corresponds to the largest Ca value of 5.6×10^{-3} and the smallest receding angle Θ_{ext} of 33.6° reached in this study, which shows that no viscous deformation of the meniscus was detected for any of the systems at the magnification used. This result is in accordance with the conclusion of Clanet and Quéré,[41] who studied the dynamics of viscous liquid rising on fibers and found that the steady meniscus shape is quasi-static.

Velocity Dependence of the Extrapolated Dynamic Contact Angle. Figure 2 shows the dependencies of the extrapolated dynamic contact angle, further denoted as Θ, on the contact line velocity V, for methanol, ethanol, 1-butanol, and 1-octanol. The advancing branches at $V > 0$ display similar small increases of Θ; for the same velocity range from 0 to 2 cm/s, the maximum difference $\Theta - \Theta_A$ is 5° for methanol and 9° for octanol. The receding Θ/V dependencies are stronger and more specific; the maximum difference $\Theta - \Theta_R$ is 9° for methanol and 28° for octanol. The asymmetry of the wetting and dewetting branches increases from methanol toward octanol, correlating with a decrease of the characteristic hydrodynamic velocity γ/μ at which viscous and capillarity effects become comparable (see Table 1). This correlation implies a hydrodynamic origin of the asymmetry. In the advancing mode, Θ monotonically increases for all liquids. A monotonic trend is also observed for the receding mode of methanol and ethanol whereas butanol and octanol exhibit S-shaped receding Θ/V branches in the same velocity range. The existence of an inflection in these dependencies suggests a transition between two different mechanisms.

IV. Comparison between Theory and Experiment

Hydrodynamic Theories. The quasi-static form of the dynamic meniscus implies the equivalence of different definitions of the macroscopic dynamic contact angle. Under such conditions, hydrodynamic eqs 1−6 require linear Θ^3/Ca plots if $\Theta_c = $ a constant. Figure 3 shows our experimental data on this characteristic hydrodynamic scale. Linearity is observed in all dependencies except for their initial sections, where the variation of Θ^3 with Ca is stronger. Table 3 shows that the minimum capillary numbers, above which the Θ^3/Ca plots become linear, are almost the same, $|Ca_{\min}| \approx (1 \div 5) \times 10^{-3}$. The prediction of eq 1a of equal slopes of the advancing and receding branches is fulfilled only for methanol; for butanol and octanol, $d\Theta_{\text{rec}}^3/dCa$ and $d\Theta_{\text{adv}}^3/dCa$ differ considerably from each other. The maximum slip lengths $L_{S,\max}$ evaluated from these slopes and eq 7 have unrealistic dimensions, which also suggests that eq 1a does not adequately describe the experimental data.

The wetting−dewetting asymmetry of the advancing and receding branches of butanol and octanol could be formally related to different signs and/or values of C_{ZS} for $Ca > 0$ and $Ca < 0$ in eq 3a. Using a physically acceptable value for $\ln(L_H/L_S) = 12$ for both the wetting and dewetting modes and
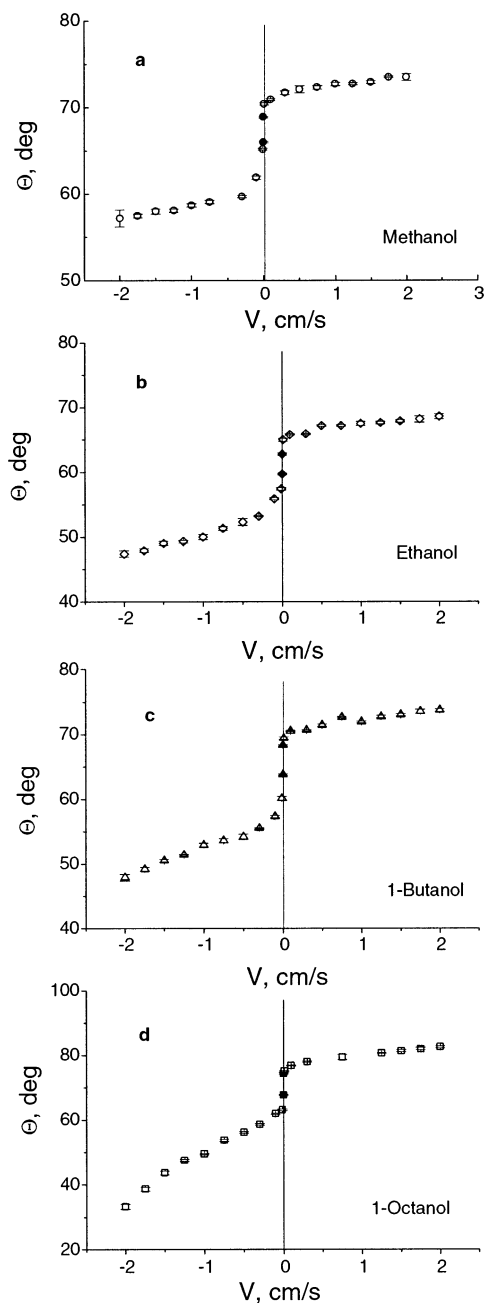
Figure 2. Dependencies of the extrapolated dynamic contact angle θ on the contact line velocity V for methanol, ethanol, 1-butanol, and 1-octanol. The solid points correspond to the static advancing and receding contact angles.

Figure 3. Presentation of the experimental data from Figure 2 on the characteristic hydrodynamic scale θ^3 vs Ca. The static values of θ_A^3 and θ_R^3 are shown with solid points.

assuming that C_{ZS} differs only in sign, we find that $C_{ZS} = \pm 1.6$ for butanol and $C_{ZS} = \pm 4.2$ for octanol. The plus sign stays for receding, and the minus sign, for advancing liquid. This result would mean that the asymmetry of the Θ^3/Ca dependence is due to the asymmetry of the inner-region dynamics. Such a conclusion contradicts the two-region solution of Kafka and Dussan,[43] which introduces a particular slip law into the model:

$$\Theta_{ext} = \Theta_c + 1.273 Ca \left[\ln\left(\frac{(\gamma/\rho g)^{1/2}}{L_S} \right) + 0.550 \right] \quad (27)$$

Equation 27 predicts equal slopes of the advancing and receding Θ_{ext}/Ca dependencies for the same air−liquid−solid system. Therefore, the two-region hydrodynamic model cannot explain the wetting−dewetting asymmetry when the inner zone is handled explicitly.
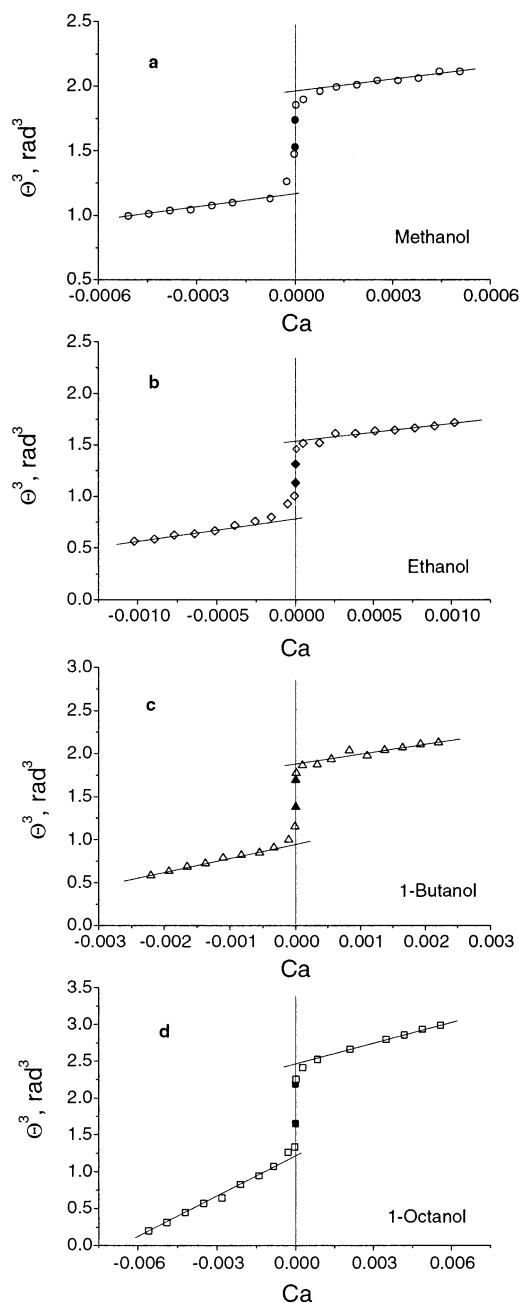
The geometry constant C_V introduced by Voinov[4] is independent of the properties of the liquid and the direction of the contact line motion. However, an estimation of C_V from Table 3 and eq 4 with $\ln(L_H/L_S) = 12$ gives different values of C_V for butanol and octanol. Different values are obtained also for the advancing and receding of the same liquid: $C_{V,adv} = 3.3$, $C_{V,rec} = 6.4$ for butanol, and $C_{V,adv} = 0.2$, $C_{V,rec} = 8.5$ for octanol. Such a dependence of C_V on the properties of the liquid and on the sign of Ca contradicts eq 4. Moreover, our values of C_V are too large as compared to those of Voinov, ranging from 1.0 to 1.8.

Instead of a reasonable value of $\ln(L_H/L_S)$, we could use the maximum values of $C_{ZS} = -3.0$ and $C_V = 1.8$ reported in the literature.[4,14] By substituting them into eq 5, we calculated the maximum slip lengths for the liquids used. The obtained values of $L_{S,max}$ are better as those in Table 3; $L_{S,max} = 8 \times 10^{-7}$ cm

Partial Wetting/Dewetting in Well-Defined Systems

J. Phys. Chem. B, Vol. 107, No. 7, 2003 **1641**

TABLE 3: Comparison of the Parameters of the Linear Fit of the Hydrodynamic Theory Obtained from the Plot of Θ^3 vs Ca in Figure 3

liquid	Ca_{min}^{rec}	Ca_{min}^{adv}	$(d\Theta_{rec}^3/dCa)$	$(d\Theta_{adv}^3/dCa)$	$L_{s,max}$ (receding) [cm]	$L_{s,max}$ (advancing) [cm]
methanol	-1×10^{-3}	1×10^{-3}	346 ± 42	332 ± 23	5.3×10^{-19}	2.3×10^{-18}
ethanol	-2×10^{-3}	2×10^{-3}	271 ± 18	238 ± 24	2.1×10^{-15}	8.6×10^{-14}
1-butanol	-3×10^{-3}	2×10^{-3}	166 ± 6	138 ± 9	2.6×10^{-10}	5.8×10^{-9}
1-octanol	-5×10^{-3}	4×10^{-3}	185 ± 4	110 ± 4	3.1×10^{-11}	1.3×10^{-7}

for butanol and 1.5×10^{-5} cm for octanol. However, the values of $L_{S,max}$ for methanol and ethanol remain subatomic. Molecular dynamics simulations[44] show that L_S slightly exceeds the dimensions of liquid molecules, and this result could serve as a reference. Therefore, eq 5 also disagrees with our experimental data. This implies that a three-region solution explicitly giving the terms $Q_{in}/f(\Theta_c)$ and $Q_{out}/f(\Theta_m)$ in eq 2 is necessary.

The existence of initial nonlinear sections of the Θ^3/Ca plots shows that the assumption that Θ_c = a constant is not realistic. Zhou and Sheng[14] showed that a $\Theta_c(Ca)$ dependence causes a stronger variation of the macroscopic dynamic angle at $Ca < 10^{-2.7} = 2.0 \times 10^{-3}$. This limit coincides with our Ca_{min} values from Table 3. This coincidence motivates the use of eqs 9a and 9b, which introduce a $\Theta_c(Ca)$ dependence. The receding branches were fitted with $\Theta_0 = \Theta_R$, and the advancing ones, with $\Theta_0 = \Theta_A$. Figure 4 shows the fits with B, n, and $H = \ln(L_H/L_S) + C_{ZS} - C_V$ set as free parameters. The good coincidence between the theoretical and experimental trends qualitatively supports eqs 9a and 9b. However, it does not prove the particular mechanism of the contact line friction proposed in ref 14; for this purpose, one should look at the variation of B, n, and H with the properties of the liquid (Table 4). For the receding mode, B and n decrease from methanol toward octanol with n remaining within the limits $0 < n < 0.5$ reported in the literature.[14,45] Nonrepresentative values of H_{rec} (very large errors) were obtained for methanol and ethanol, but for butanol and octanol, H_{rec} was well-defined. The receding values of B qualitatively follow the dependence predicted by eq 10. Moreover, substitution of B_{rec} in eq 10 gives reasonable distances between surface defects L_d, which do not systematically change from methanol toward octanol (Table 4). In contrast to this, the variation of B_{adv} with liquid properties is opposite to that expected from eq 10, and the values of L_d are smaller by 2 orders of magnitude, as for receding. Such a dependence of L_d on the direction of the contact line motion and the opposite variation of B and n for wetting and dewetting modes are so far unclear and need further investigation.

Molecular-Kinetic Theories. Figure 5 presents our experimental data on the $\cos \Theta$ versus Ca scale. According to eq 16, such a plot requires symmetric branches for $Ca > 0$ and $Ca < 0$. As one can see, an approximate symmetry exists for methanol, where the solid line representing the molecular-kinetic theory satisfies almost all data points. However, the experimental data in Figure 5b–d have clearly asymmetric trends. This fact does not enable a simultaneous fit of eq 16 to the whole $\cos \Theta/Ca$ dependence. To obtain unique values of λ, $K_{0,S}$, and Θ_0 for ethanol, butanol, and octanol, we fitted eq 16 simultaneously for wetting and dewetting but over a limited Ca range. The solid lines in Figure 5b–d were obtained by eliminating the final experimental points and repeating the fit until a minimum chi-squared value was achieved. The static values of $\cos \Theta_R$ and $\cos \Theta_R$ were excluded from the fit.

The maximum receding and advancing capillary numbers, above which the experimental points begin to deviate from the theoretical curve, are shown in Table 5. It is curious that all of the obtained values are below or close to the Zhou–Sheng[14]

limit, $|Ca| = 2.0 \times 10^{-3}$. This implies that at $Ca < Ca_{max}$ the energy dissipation is located in the vicinity of the wetting perimeter and could be evaluated by the molecular-kinetic theory. However, the receding Ca_{max} values are smaller than the advancing Ca_{max} values (Table 5), which contradicts the molecular-kinetic model.

Table 5 gives the free parameters λ and $K_{0,S}$ that were determined from the partial fits in Figure 5. The values of λ
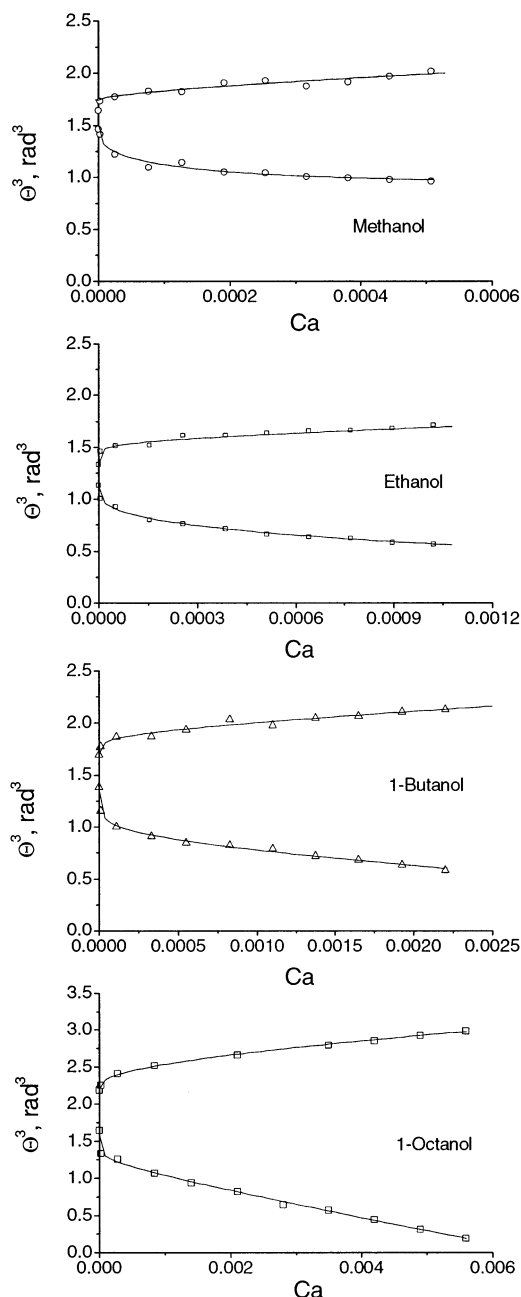

Figure 4. Fits of eqs 9a and 9b representing Zhou–Sheng–Voinov theory to our data on the θ^3/Ca scale. Advancing and receding branches were treated separately. In both modes, Ca is taken to be positive because of the noninteger power n in eq 8.

TABLE 4: Comparison of the Free Parameters of the Fit of Equations 9a and 9b to the Receding and Advancing Branches of the Θ^3/Ca Plots in Figure 4

	receding				advancing			
liquid	B	n	H	L_d [cm]	B	n	H	L_d [cm]
methanol	1.94 ± 1.49	0.31 ± 0.08		1.3×10^{-7}				
ethanol	1.49 ± 0.44	0.31 ± 0.03		2.8×10^{-7}	0.18 ± 0.07	0.14 ± 0.04	10.9 ± 5.1	4.4×10^{-9}
butanol	0.49 ± 0.10	0.18 ± 0.02	9.7 ± 2.1	1.7×10^{-7}	0.23 ± 0.19	0.22 ± 0.09	7.6 ± 4.6	3.7×10^{-8}
octanol	0.28 ± 0.08	0.15 ± 0.04	17.8 ± 1.3	3.8×10^{-8}	0.67 ± 0.30	0.36 ± 0.05	3.9 ± 2.2	2.2×10^{-6}

range between 4 and 6 nm, thus exceeding the molecular dimensions by an order of magnitude. The oscillation frequency $K_{0,S}(1)$ evaluated from the simple molecular-kinetic theory decreases from about 2 kHz for methanol to 100 Hz for octanol. The values of $K_{0,S}(2)$ estimated from the more general expression for C_B are on the order of 10^5 Hz. The more general version gives a higher oscillation frequency of the molecules at the

Figure 5. Presentation of our experimental data on the cos θ/Ca scale, which is characteristic of the molecular-kinetic theory. The solid lines show the fits of eq 16 to the part of the advancing and receding data giving minimum chi-squared values (see the text).

contact line because it also accounts for the viscous dissipation in its vicinity.

In fact, one should use the Θ_0 data from Table 2 to reduce the number of free parameters in eq 16. However, this leads to more significant disagreement between theory and experiment, so we determined Θ_0 from the fit. The obtained values exceed those in Table 2 by less than 1.5°. The improving effect of such a small difference suggests that eq 16 is very sensitive to Θ_0. The disagreement could result from the values of Θ_A and Θ_R, which were read after 1-min meniscus relaxation. Instead of them, the limiting static contact angles $\Theta_{A,max}$ and $\Theta_{R,min}$ should be substituted into eq 25 to calculate Θ_0 correctly.

Combined Molecular-Hydrodynamic Theory. Figure 6 presents the fits of eqs 24a and 24b to our experimental data on the corresponding theoretical Θ/Ca scale. One can see that the molecular-hydrodynamic theory represents the whole variation of the experimental advancing and receding contact angles. The coincidence between theory and experiment in the dewetting mode is quantitative for all liquids. Even the S shape of the receding branches observed for butanol and octanol is well modeled by the theory. This fact suggests that the inflections in these branches could be referred to the transition from the contact line to bulk viscous friction. Such an explanation was proposed for other systems in our previous publications.[11,13,16] For the advancing branches, the theoretical and experimental trends are slightly different, but the qualitative agreement is quite fair. The wetting−dewetting asymmetry is reproduced by the molecular-hydrodynamic theory, although for the most extreme case, shown in Figure 6d, the agreement is semiquantitative.

The ability of the theory to describe completely the Θ/Ca dependencies yields representative values of the free parameters, which do not depend on the direction of the contact line motion. Table 6 shows λ, $K_{0,S}$, H, and Θ_0, which were obtained from the fits. The values of λ for all liquids coincide within the error limits, giving an average value of $\lambda = 6.0 \pm 0.6$ nm. Unfortunately, the errors of determination for $K_{0,S}(1)$ and $K_{0,S}(2)$ for methanol, ethanol, and butanol exceed the mean values, which should be considered to be estimates of the order of magnitude. Despite this, it is clear that the simple molecular-hydrodynamic theory gives unreasonably small values of $K_{0,S}(1)$ for butanol and octanol. The more general molecular-hydrodynamic theory yields more-acceptable values of $K_{0,S}(2)$ probably because it accounts for the energy dissipation more completely. $K_{0,S}(2)$ decreases from 10^4 to 10^2 Hz from methanol to octanol, as one would expect from the increasing molecular volume. The value of $H = \ln(L_{0,R}/L_C) - C_V$ does not systematically change from liquid to liquid, in qualitative agreement with the molecular-hydrodynamic theory. Because of the constant geometry of the studied systems, Voinov constant C_V should have the same value for all liquids. The logarithmic term should be practically constant because $L_{0,R} \approx$ a constant (Table 2) and L_C cannot significantly change from methanol to octanol. However, the mean value of $H = 19.7 \pm 3.0$ is too high. With a reasonable cutoff length of $L_C = 10^{-7}$ cm, one obtains $C_V = 7.3 \pm 3.0$, which considerably exceeds the value of $C_V = 1.0 \div 1.8$ reported by Voinov for drops, slots, and capillaries.[4,26] This fact
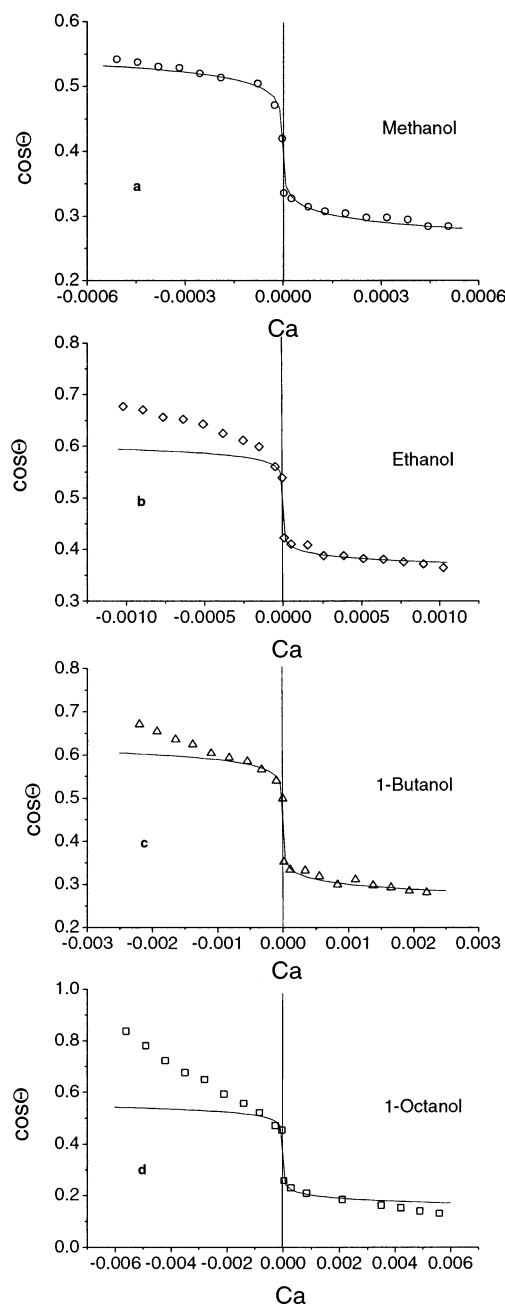
Partial Wetting/Dewetting in Well-Defined Systems

J. Phys. Chem. B, Vol. 107, No. 7, 2003 **1643**

TABLE 5: Comparison of the Parameters of the Molecular-Kinetic Theory from the Best Fit of Equation 16 to the Data in Figure 5[a]

liquid	Ca_{max} receding	Ca_{max} advancing	λ [nm]	$K_{0,S}(1)$ [s^{-1}][b]	$K_{0,S}(2)$ [s^{-1}][c]	Θ_0 [deg]
methanol	-4×10^{-4}	$>0.5 \times 10^{-3}$	4.8 ± 0.3	$(1.9 \pm 1.3) \times 10^3$	$(1.1 \pm 0.8) \times 10^5$	66.2 ± 0.2
ethanol	-1.5×10^{-4}	$>1 \times 10^{-3}$	5.9 ± 0.3	$(9.9 \pm 9.5) \times 10^1$	$(1.6 \pm 1.5) \times 10^4$	61.1 ± 0.2
1-butanol	-5×10^{-4}	$>1.6 \times 10^{-3}$	4.4 ± 0.2	$(3.8 \pm 3.2) \times 10^2$	$(2.4 \pm 2.0) \times 10^5$	63.6 ± 0.2
1-octanol	-5×10^{-4}	2×10^{-3}	4.2 ± 0.4	$(1.0 \pm 2.4) \times 10^2$	$(3.0 \pm 7.3) \times 10^5$	69.2 ± 0.3

[a] The fits were obtained via the consecutive omission of the final left and right points until a minimum chi-squared value was achieved. [b] $K_{0,S}(1) = (C_B\gamma/2\lambda\mu)$. [c] $K_{0,S}(2) = (C_B\gamma v/2\lambda h)$.
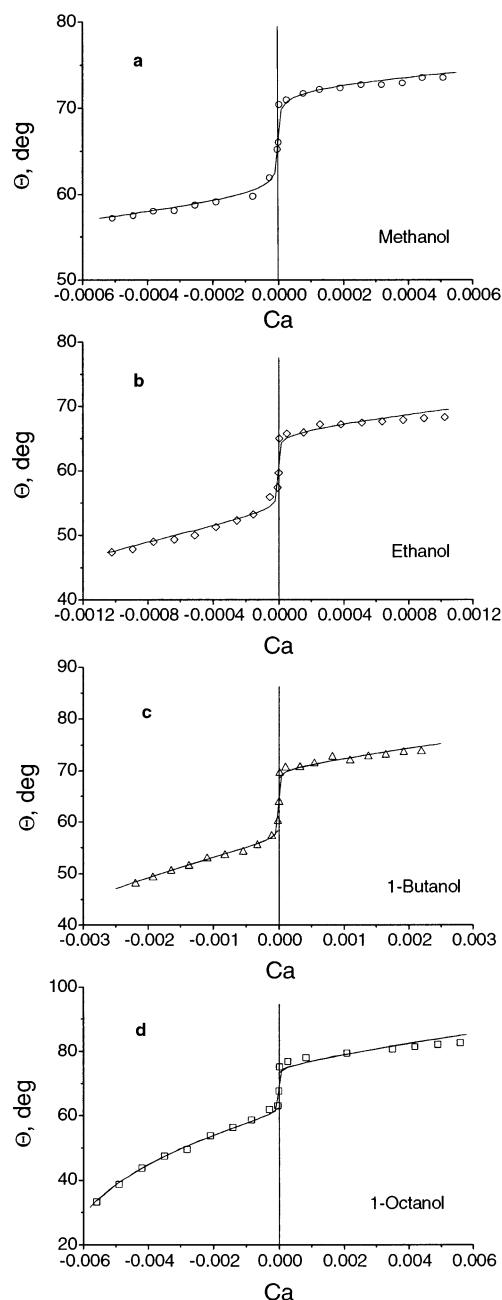
Figure 6. Fits of eqs 24a and 24b of the molecular-hydrodynamic theory to our experimental data on the corresponding θ/Ca scale. The solid lines represent simultaneous fits to all of the advancing and receding dynamic contact angles.

implies shortcuts of the molecular-hydrodynamic theory that should be a matter of further investigation.

Comparison of Theory and Experiment for Complete Wetting. Dussan, Rame, and Garoff[7] published an investigation of complete wetting for a range of capillary numbers,

TABLE 6: Comparison of the Parameters of the Molecular-Hydrodynamic Theory Obtained from the Best Fit of Equations 24a and 24b to the Data in Figure 6

liquid	λ [nm]	$K_{0,S}(1)$ [s^{-1}][a]	$K_{0,S}(2)$ [s^{-1}][b]	H[c]	Θ_0 [deg]
methanol	5.4 ± 0.6	605 ± 1020	$(3.5 \pm 5.8) \times 10^4$	20.7 ± 12.2	66.2 ± 0.2
ethanol	6.4 ± 1.0	29 ± 73	$(4.8 \pm 12) \times 10^3$	23.2 ± 5.2	60.0 ± 0.2
1-butanol	6.2 ± 0.8	2.5 ± 7.5	$(1.6 \pm 4.7) \times 10^3$	15.5 ± 2.0	63.5 ± 0.2
1-octanol	6.2 ± 0.3	0.17 ± 0.03	$(5.0 \pm 0.8) \times 10^2$	18.4 ± 1.2	68.0 ± 0.3

[a] $K_{0,S}(1) = (C_B\gamma/2\lambda\mu)$. [b] $K_{0,S}(2) = (C_B\gamma v/2\lambda h)$. [c] $H = \ln((L_{0,R}/L_c)) + C_V$.
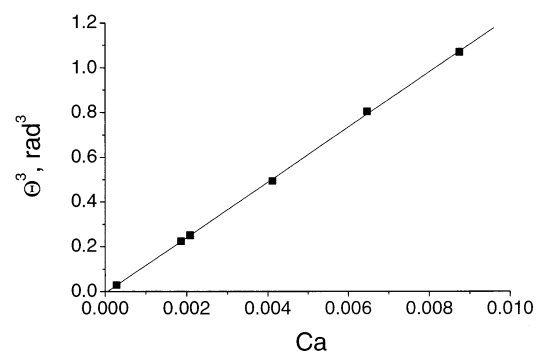
Figure 7. Plot of θ^3 vs Ca for the extrapolated dynamic contact angle obtained in ref 7 for a glass tube being immersed in silicon oil at different velocities. The excellent straight line, zero intercept, and realistic $L_{S,max}$ value confirm the hydrodynamic theory for complete wetting.

$2.8 \times 10^{-4} - 8.3 \times 10^{-2}$, which partially overlaps with ours. A glass tube was immersed in silicon oil at a constant speed and tilt angle. The coordinates of the meniscus profile were determined possibly close to the contact line, where the matched solution for the intermediate and outer regions holds. Fitting this solution to the experimental dependence $\Theta(r)$ of the slope of the fluid interface Θ at a distance r from the contact line, they found excellent agreement between theoretical and experimental profiles and obtained Θ_{ext} as a single free parameter of the fit.

The values of Θ_{ext} thus obtained are plotted in Figure 7 for the characteristic hydrodynamic scale Θ_{ext}^3 versus Ca. All experimental points fall on an excellent straight line with a correlation coefficient of $R = 0.9998$. As expected, the intercept is zero because for complete wetting $\Theta_c = \Theta_{ext}(Ca = 0) = 0°$. The slope gives $H = \ln(L_H/L_C) - C_V = 13.66$. An evaluation of the slip length from eq 7 with $L_H = (\gamma/\rho g)^{1/2}$ and $C_V = 0$ gives $L_C = 1.7 \times 10^{-7}$ cm. Taking the maximum value of $C_V = 1.8$ found by Voinov decreases L_C to 2.8×10^{-8} cm, but both values remain physically reasonable. This shows that the theoretical profile of the fluid interface and the velocity dependence of the extrapolated dynamic contact angle predicted by the hydrodynamic theory for complete wetting are in quantitative agreement with the experiment.

Similar results were obtained by Redon, Brochard-Wyart, Hervet, and Rondelez[46] for the spreading of large PDMS drops

on smooth silicon wafers. The hydrodynamic theory for this particular case was proven by comparing the theoretical and experimental profiles of the drops and checking the velocity dependence of the dynamic contact angle. The latter was linearized on the Θ^3/V scale passing through the zero point and giving reasonable H values.

However, Marsh, Garoff, and Dussan[47] performed a study of an air−silicon oil−glass system where the geometry was varied through the tilt of the glass tube. Instead of Θ_{ext}, a complex microscopic parameter $L = L_S[\exp(-\Theta_c/9Ca)]$ was determined from the fit of the theoretical and experimental meniscus profiles. Figure 4[47] shows that L is not constant, although $\Theta_c = 0°$ for complete wetting and the above definition gives $L = L_S$. The obtained values of L_S are reasonable, but they decrease from 10^{-4} cm to 1×10^{-6} cm, reaching a plateau at $Ca = 3.5 \times 10^{-3}$. Such a dependence of the slip length on the capillary number disagrees with the considered hydrodynamic models.

V. Discussion

The experimental data in Figure 3 implies that both the friction at the contact line and in the intermediate region of the meniscus are significant. Figure 5 supports this conclusion, showing that the molecular-kinetic theory could model the contact line friction at $Ca < \pm 5 \times 10^{-4}$. The present results for the wetting and dewetting of a well-defined solid surface by pure liquids confirm our previous conclusion[11,13,16,31] that dissipation at the contact line predominates at low velocities and bulk viscous dissipation becomes more important at high contact line speeds. An increase of the viscous effects with increasing capillary number is natural, but the asymmetry of these effects for the wetting and dewetting modes is nontrivial. Such asymmetry could be due to the opposite changes of the receding and advancing dynamic angles with increasing $|Ca|$ Applying eq 17 to the same three-phase system, one finds that different values of Θ_{rec} and Θ_{adv} at the same capillary number $Ca*$ yield larger viscous contributions for receding because the denominator of the first term $\Theta_{rec}(-Ca*)$ is smaller than $\Theta_{adv}(+Ca*)$. For dewetting, eq 17 correctly predicts an increase of the viscous dissipation with increasing velocity because $\Theta_{rec}(Ca)$ is a decreasing function. In the wetting mode, however, one should expect weaker viscous effects at high velocities because Θ_{adv} increases with Ca. Our Figures 3 and 5 and Tables 3 and 5 show that in both wetting and dewetting modes the molecular-kinetic theory works at low velocities and the hydrodynamic theory better fits the data at high contact line speeds.

The asymmetry of the wetting and dewetting modes increases from ethanol toward octanol in correlation with decreases of the characteristic hydrodynamic velocity γ/μ. This fact suggests that it has a hydrodynamic origin. However, asymmetry could result from different dynamic behaviors of the contact line or/and the inner region at advancing and receding.[4] The more general molecular-hydrodynamic theory applied in this study assumes that both the contact line and inner-region friction do not depend on the direction of motion. The successful fit of eqs 24a and 24b to both the $Ca < 0$ and $Ca > 0$ branches (Figure 6) implies that this theory contains intrinsic asymmetry that is not due to different values of λ, K_0, and H for wetting and dewetting. The values of the parameters in Table 6 characterize the whole Θ/Ca dependence and are unique for the given system. Therefore, the wetting−dewetting asymmetry results from different distributions of the energy dissipation for the advancing and receding of the same liquid on the same solid

surface. Such a scenario explains the deviation of the molecular-kinetic theory from experimental data at different positive and negative Ca_{max} values (Figure 5 and Table 5). This means that the viscous dissipation in the intermediate region becomes comparable with the dissipation in the contact line zone at different capillary numbers for the wetting and dewetting modes.

The unreasonable slip or cutoff lengths in Tables 3 and 6 cannot be explained by the hydrodynamic and molecular-hydrodynamic theory. The large values of λ significantly exceeding molecular dimensions are inconsistent with the molecular-kinetic theory. These facts indicate shortcuts of all of the considered theoretical models. Their appearance even for well-defined systems implies that further theoretical development is necessary, especially for the case of partial wetting.

Our conclusion is not universal. Redon, Brochard-Wyart, and Rondeles[48] studied the expansion of dry patches in alkane films on hydrophobized silicon wafers. Such systems also exhibit partial wetting ($\Theta_0 = 15° \div 36°$) and are very well defined. The Si wafers are smooth, and their modification via the chemisorption of long-chain amphiphils retained the original smoothness, reducing the surface energy. The nonpolar pure liquids that were used have low surface tension, and their characteristic hydrodynamic velocities γ/μ ranging between 3200 and 830 are close to ours (cf. Table 1). Negligible hysteresis of the static contact angle (below 2°) was found for all systems. The measured time-dependence of the dry-patch radius $R(t)$ confirmed the hydrodynamic theory in many aspects: $R \sim t$, $dR/dt \sim \Theta_0^3$, and $dR/dt \sim 1/\mu$. The same value of $H = 6.0 \div 6.3$ was obtained for all of the studied alkanes, in agreement with the theoretical prediction that $H = \ln(L_H/L_S)$ does not depend on the properties of the liquid. Substituting this value into eq 7 and taking the height of the liquid rim formed in front of the contact line as $L_{H,max} = 0.1$ cm, one finds a reasonable value for $L_{S,max} = (1.8 \div 2.5) \times 10^{-4}$ cm.

References and Notes

(1) De Gennes, P. G. *Rev. Mod. Phys.* **1985**, *57*, 827.

(2) Kistler, S. F. In *Wettability*; Berg, J. C., Ed.; Marcel Dekker: New York, 1993; p 311.

(3) Dussan, E. V. *J. Fluid Mech.* **1976**, *77*, 665.

(4) Voinov, O. V. *J. Fluid Dyn. (Engl. Transl.)* **1976**, *11*, 714.

(5) Cox, R. G. *J. Fluid Mech.* **1986**, *168*, 169.

(6) De Gennes, P. G.; Hua, X.; Levinson, P. *J. Fluid Mech.* **1990**, *212*, 55.

(7) Dussan, V. E. B.; Rame, E.; Garoff, S. *J. Fluid Mech.* **1991**, *230*, 97.

(8) Blake, T. D.; Haynes, J. M. *J. Colloid Interface Sci.* **1969**, *30*, 421.

(9) Ruckenstein, E.; Dunn, C. S. *J. Colloid Interface Sci.* **1977**, *59*, 135.

(10) Glasstone, S.; Laidler, K. J.; Eyring, H. *The Theory of Rate Processes*; McGraw-Hill: New York, 1941.

(11) Petrov, J. G.; Radoev, B. P. *Colloid Polym. Sci.* **1981**, *259*, 753.

(12) Brochard-Wyart, F.; de Gennes, P. G. *Adv. Colloid Interface Sci.* **1992**, *39*, 1.

(13) Petrov, P. G.; Petrov, J. G. *Langmuir* **1992**, *8*, 1762.

(14) (a) Zhou, M. Y.; Sheng, P. *Phys. Rev. Lett.* **1990**, *64*, 882. (b) Sheng, P.; Zhou, M. Y. *Phys. Rev. A* **1992**, *45*, 5694.

(15) Shanahan, M. E. R.; de Gennes, P. G. *Adhesion 11*; Allen, K. W., Ed.; Elsevier Applied Science: London, 1987; p 71.

(16) Petrov. J. G.; Sedev, R. V.; Petrov, P. G. *Adv. Colloid Interface Sci.* **1992**, *38*, 229.

(17) Gribanova, E. V. *Adv. Colloid Interface Sci.* **1992**, *39*, 235.

(18) Cazabat, A. M. *Adv. Colloid Interface Sci.* **1992**, *42*, 65.

(19) Hayes, R.; Ralston, J. *J. Colloid Interface Sci.* **1993**, *159*, 429.

Partial Wetting/Dewetting in Well-Defined Systems

J. Phys. Chem. B, Vol. 107, No. 7, 2003 **1645**

(20) Sharpe, M. R.; Peterson, I. R.; Tatum, J. P. *Langmuir* **2002**, *18*, 3549.

(21) Drummond, C. J.; Georgaklis, G.; Chan, D. Y. C. *Langmuir* **1996**, *12*, 2617.

(22) Schneemilch, M.; Hayes, R. A.; Petrov, J. G.; Ralston, J. *Langmuir* **1998**, *14*, 7047.

(23) Schneemilch, M. Ph.D. Thesis, University of South Australia, Adelaide, Australia,1999.

(24) Johnson, R. E., Jr.; Dettre, R. H. In *Wettability*; Berg, J. C., Ed.; Marcel Dekker: New York, 1993; p 1.

(25) Drummond, C. J.; Chan, D. Y. C. *Langmuir* **1996**, *12*, 3356. Drummond, C. J.; Chan, D. Y. C. *Langmuir* **1997**, *13*, 3890.

(26) Voinov, O. V. *Sov. Phys. Dokl. (Engl. Transl.)* **1978**, *23*, 891.

(27) Wenzel, R. N. *Ind. Eng. Chem.* **1936**, *28*, 988. (b) Wenzel, R. N. *J. Phys. Colloid Chem.* **1949**, *53*, 1466.

(28) Cassie, A. B. D.; Baxter, S. *Trans. Faraday Soc.* 1**944**, *40*, 546.

(29) Petrov, J. G.; Ralston, J.; Hayes, R. *Langmuir* **1999**, *15*, 3365.

(30) Blake, T. D. In *Wettability*; Berg, J. C., Ed.; Marcel Dekker: New York, 1993; p 251.

(31) Petrov, J. G.; Petrov, P. G. *Colloids Surf.* **1992**, *64*, 143.

(32) Hayes, R.; Ralston, J. *Langmuir* **1994**, *10*, 340.

(33) Cherry, B. W.; Holms, C. M. *J. Colloid Interface Sci.* **1969**, *29*, 174.

(34) Petrov, J. G. To be submitted for publication.

(35) Adam, N. K. *Adv. Chem. Ser.* **1964**, *43*, 53.

(36) Andrieu, C.; Sykes, C.; Brochard-Wyart, F. *Langmuir* **1994**, *10*, 2077.

(37) Decker, E. L.; Garoff, S. *Langmuir* **1996**, *12*, 2100.

(38) Lam, C. N. C.; Wu, R.; Li, D.; Hair, M. L.; Neumann, A. W. *Adv. Colloid Interface Sci.* **2002**, *96,* 169.

(39) Huh, C.; Scriven, L. E. *J. Colloid Interface Sci.* **1971**, *35*, 85.

(40) Derjaguin, B. V. *Dokl. Akad. Nauk SSSR* **1946**, *51*, 517.

(41) Petrov, J. G.; Sedev, R. V. *Colloids Surf.* **1993**, *74*, 233.

(42) Claret, C.; Quéré, D. *J. Fluid Mech.* **2002**, *460*, 131.

(43) Kafka, F. Y.; Dussan, V. E. B. *J. Fluid Mech.* **1979**, *95*, 539.

(44) Thompson, P.; Robbins, M. *Phys. World* **1990**, *3*, 35.

(45) Stokes, J. P.; Higgins, M. J.; Kushnick, A. P.; Bhattacharya, S.; Robbins, M. O. *Phys. Rev. Lett.* **1990**, *65*, 1885.

(46) Redon, C.; Brochard-Wyart, F.; Hervet, H.; Rondelez, F. *J. Colloid Interface Sci.* **1992**, *149*, 580.

(47) Marsh, J.; Garoff, S.; Dussan, E. V. *Phys. Rev. Lett.* **1993**, *70*, 2778.

(48) Redon, C.; Brochard-Wyart, F.; Rondelez, F. *Phys. Rev. Lett.* **1991**, *66*, 715.